Analyst

RSC Publishing

PAPER

View Article Online
View Journal | View Issue

Cite this: *Analyst*, 2013, **138**, 2357

Non-destructive enhancement of latent fingerprints on stainless steel surfaces by electrochemiluminescence†

Linru Xu, Yan Li, Yayun He and Bin Su*

Received 15th January 2013
Accepted 18th February 2013

DOI: 10.1039/c3an00110e

www.rsc.org/analyst

Visualization and detection of latent fingerprints (LFPs) on metal surfaces are of highly practical importance, *e.g.*, in identifying gun cartridges. We report herein the visualization of LFPs on stainless steel surfaces by electrochemiluminescence (ECL). Since organic residues, such as fatty acids, in the fingerprint deposit make the underlying surface electrochemically inert or less active, an ECL reaction occurs only on the metal portions untouched by the fingertip, hence generating a negative image of the fingerprint. The popular ECL reaction solution, consisting of ruthenium(II) tris(2,2′-bipyridyl) and tri-*n*-propylamine, was used for this imaging purpose. Factors, including the applied potential and the concentration of ECL luminophore, as well as the stability of ECL negative images, were investigated to achieve a satisfactory visualization enhancement. This imaging approach is simple, rapid, non-invasive, and no pre-treatment either on the background or on the fingerprint itself is needed. It constitutes a powerful tool for visualizing LFPs on metal surfaces. This method was also demonstrated to be suitable for enhancing LFPs collected from various surfaces.

Introduction

When a fingertip is brought into contact with an object, a contour impression of the fingertip ridge pattern will be deposited on the object surface. Fingerprint materials are composed of perspiration substances secreted by the eccrine glands and sebaceous residues, such as fatty acids, picked up by the fingertips from the face or scalp. As each fingerprint is truly unique, invariable for an individual and cannot be easily forged, it functions as an indispensable tool in forensic investigations, as well as in our daily life for many other purposes such as safety control, individual credentials[1–3] and even chemical analysis.[4–13]

However, most fingerprints are invisible to naked eyes (termed latent fingerprints, LFPs) and require some means of "development" to enhance the visual contrast between the deposited ridge pattern and the background surface. The majority of developments rely upon using suitable chemical agents to interact with ridge materials to achieve an adequate visual contrast against the background surface.[14] However, difficulties often arise in particular for LFPs embedded on a multicoloured or dark background, for those left on porous surfaces, for those aged due to degradation and volatility of the sebaceous components or for those contaminated with body fluids or other components. In addition, such a development is also invasive and destructive, obstructing or even completely preventing subsequent analysis, *e.g.* chemical identification and DNA profiling.[15]

Non-destructive visualization of LFPs can be achieved in a reverse manner by developing the substrate surface instead of the ridge pattern. In this case, the ridge pattern functions as an inert template or mask. For example, vapour phase deposition of gold and then zinc under vacuum remains to be the most sensitive technique for developing a negative image for LFPs on nonporous surfaces.[16–19] For LFPs on paper surfaces, they can be also enhanced in a negative mode by using gold nanoparticles capped by chemical agents with preferential affinity for paper, in conjunction with using the traditional silver physical developer.[20] Selective deposition of electrochromic polymer on the background surface is also able to enhance the fingerprint details by tuning the colour and optical density upon applying an external voltage.[21–24] Recently, we have reported the primary results on visual enhancement of LFPs by electrochemiluminescence (ECL). In a typical ECL reaction solution containing ECL generating luminophore, *e.g.*, ruthenium(II) tris(2,2′-bipyridyl) ($Ru(bpy)_3^{2+}$), and a co-reactant species, *e.g.*, tri-*n*-propylamine (TPrA), sebaceous fingerprints deposited on the surface of indium tin oxide coated glasses can be enhanced directly with a satisfactory visual contrast. The sebaceous fingerprint containing sufficient amounts of organic species functions as an inert or "insulating" mask, therefore ECL is generated only from the uncovered regions of the substrate under an appropriate voltage, eventually producing a negative image (as shown in Fig. 1).[25]

Institute of Microanalytical Systems, Department of Chemistry, Zhejiang University, Hangzhou 310058, China. E-mail: subin@zju.edu.cn; Fax: +86 571 88273572; Tel: +86 571 88273496

† Electronic supplementary information (ESI) available. See DOI: 10.1039/c3an00110e

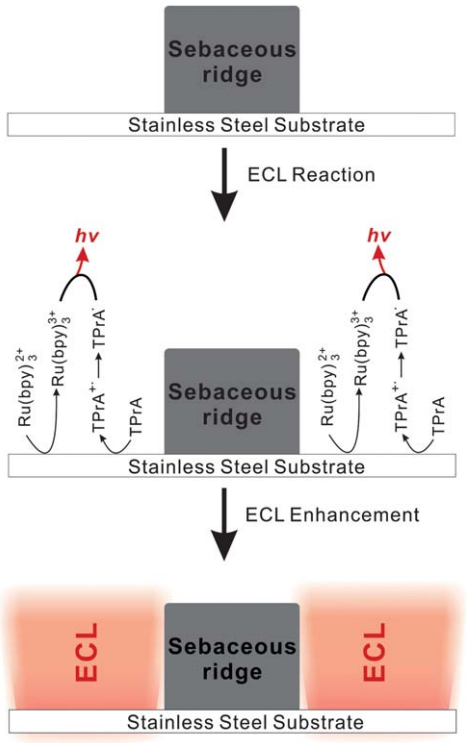

Fig. 1 Reverse enhancement of latent fingerprint by ECL.

Herein, we report the further utilization of ECL to enhance the visualization of LFPs on a metal surface, with stainless steel as a typical example. Detection of LFPs on metal surfaces is highly important and practically useful, because many crimes nowadays involve metal objects, such as door handles, guns, bullets, cartridges and knives.[21,26] Among numerous methods, electrochemistry has evolved as an interesting and valuable tool, considering its ability of manipulating the chemical reactivity of metal surfaces. Apart from the aforementioned electrochromism and ECL, electrochemical surface plasmon resonance,[27] scanning electrochemical microscopy[28–31] and scanning Kelvin probe techniques[26,32] have also been introduced to visualize LFPs on metal surfaces. In addition, many aqueous electroplating solutions and redox reagents have been previously employed to react electrochemically with the metal surface exposed between ridge deposits.[33–38]

In this work we explore the experimental details to figure out the optimal conditions for achieving a satisfactory ECL enhancement of LFPs on metal surfaces. The widely used $Ru(bpy)_3^{2+}$-TPrA ECL system was employed. Several factors, including $Ru(bpy)_3^{2+}$ concentration, applied voltage and image stability, have been studied. As we shall show, ECL is very competitive with existing methods for enhancing LFPs on metals and those collected from different object surfaces. Since no pre-treatment either on the background or on the fingerprint itself is needed, this approach is rapid, simple and non-destructive. The non-destructive nature also makes the approach valuable as it does not prevent further chemical identification, DNA analysis and so on.

Experimental

Chemicals and materials

All chemicals were used as received without further treatment. Ultrapure water (>18.2 MΩ cm) purified by a Millipore system was used throughout the experiments. Tris(2,2′-bipyridyl) ruthenium(II) dichloride hexahydrate ($Ru(bpy)_3Cl_2 \cdot 6H_2O$) was purchased from Strem Chemicals (Newburyport, USA). Tri-*n*-propylamine (TPrA) was brought from Aladdin Chemicals (Shanghai, China). A common stainless steel plate was cut into small sheets (25×50 mm^2) for supporting fingerprints. Prior to use, the sheets were cleaned by sonication for 15 min sequentially in acetone, ethanol and water, and then thoroughly rinsed with water and dried under an argon stream.

Fingerprint samples

Sebaceous fingerprints were collected from volunteers by gently rubbing their fingertips over their forehead and nose, then pressing the surfaces of the stainless steel sheet with a minimal pressure.

For the collection of LFPs from different object surfaces, a piece of double sided adhesive tape was pressed slowly onto the fingerprint deposited on the test object to ensure that there were no air bubbles present in between. The tape was then removed slowly and transferred onto a stainless steel sheet by softly pressing the tape on the sheet's surface. The test objects included a computer screen, optical disk, laboratory cabinet, and coin. All the objects surfaces were cleaned with alcohol prior to fingerprint deposition.

Electrochemistry cell and ECL imaging instrumentation

The three-electrode electrochemical cell for ECL imaging is illustrated in Fig. 2a. A stainless steel sheet carrying a fingerprint functioned as the working electrode. The electrode that faced upward was firstly fixed on a round Teflon support (bottom support), which containing a groove with the width and depth well-matched with the size and thickness of the stainless steel sheet. Then the bottom Teflon support was tightly fixed to

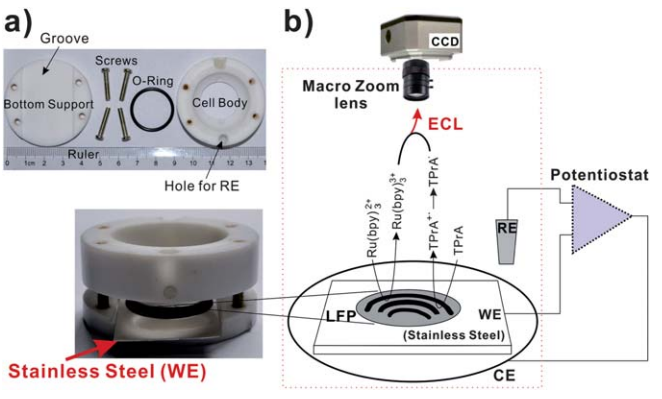

Fig. 2 (a) Photographic illustration of electrochemical cell elements (upper) and construction (lower) for ECL imaging experiment. The geometries are compared with a ruler. (b) Diagram of the ECL imaging instrumentation. The red dashed square refers to the enclosed compartment in the dark box.

the Teflon cell body *via* four screws and an O-ring. The Teflon cell body defined a volume of ~5 mL and a working electrode surface area of 3.14 cm^2. On the side wall of the cell body, a conduit was drilled for holding the silver/silver chloride (Ag/AgCl/3 M KCl) reference electrode. And the counter electrode was a platinum wire ring placed directly above the working electrode. The electrolyte solution was 0.01 M PBS containing 0.15 M NaCl, 0.5 mM $Ru(bpy)_3^{2+}$ and 50 mM TPrA unless otherwise specified.

ECL imaging was performed using a ChemiScope 2890 chemiluminescence imaging system (Clinx Science Instruments, Shanghai) equipped with a Model MLM3X-MP Macro Zoom Iris Megapixel lens (Computar, Japan) and a highly sensitive CCD camera (Model Clinx Clx210, Finger Lakes Instrumentation) (Fig. 2b). The electrochemical cell was placed directly under the lens, with its position and distance from the lens adjusted by a three-dimensional translational stage. The external voltage was supplied by a CHI832C electrochemical workstation (Chenhua, Shanghai). The CCD exposure time was set to 500 ms, and the CCD was cooled to −30 °C. The cross-sectional analysis of CCD images was done using ImageJ software, and the maximum gray value was defined as 255 units when the image was white and as 0 unit when it was black.

ECL color videos were acquired with a homemade imaging system equipped with an Mshot MC20-C Microscope Camera (Micro-shot Technology, Guangzhou) cooled at −30 °C and a Model MLM3X-MP Macro Zoom Iris Megapixel lens (Computar, Japan). The CCD exposure time was set to 500 ms.

Electrochemistry and optical measurements

The ECL intensity–voltage response of the stainless steel sheet was measured with an Autolab 302N electrochemical workstation (Metrohm, Switzerland) and a Model CR131 photomultiplier tube (PMT, Hamamatsu Photonics) connected to the Autolab 302N *via* its auxiliary second ADC signal input ports. The PMT was biased at −800 V with an RS-1300P DC power supply (RICH, Shenzhen).

Results and discussion

Human sebum is comprised mainly of triglycerides, wax esters and squalene with some cholesterol and cholesterol esters.[39] These greasy components are usually present in an LFP. As a result, LFPs on metallic surfaces distinctly appear as inert or "insulating" marks, inhibiting the underlying surface electrochemical reactivity. ECL enhanced visual contrast was indeed accomplished by selectively glowing the bare furrows and the stainless steel surface uncovered by the fingerprint through ECL emission, eventually generating a dark ridge pattern embedded in a bright background, namely a negative image of the fingerprint (as demonstrated in Fig. 1).

In this work, $Ru(bpy)_3^{2+}$-TPrA co-reactant system was chosen for ECL imaging, given its high efficiency and well understood mechanism. ECL is generated in terms of the following reactions:[40]

$$Ru(bpy)_3^{2+} - e \rightarrow Ru(bpy)_3^{3+} \quad (1)$$

$$TPrA - e \rightarrow TPrA^{+\cdot} \rightarrow TPrA^{\cdot} + H^+ \quad (2)$$

$$Ru(bpy)_3^{3+} + TPrA^{\cdot} \rightarrow [Ru(bpy)_3^{2+}]^* + \text{products} \quad (3)$$

$$[Ru(bpy)_3^{2+}]^* \rightarrow Ru(bpy)_3^{2+} + h\nu \quad (4)$$

Fig. 3a displays ECL enhanced images of an LFP on a stainless steel substrate. Apparently, the spatial pattern of a fingerprint is clearly resolved, in which the dark ridge deposits contrasted remarkably with the bright substrate for visualization. The second-level details, such as the ridge lake, termination, crossover and bifurcation could be recognized (Fig. 3a). These second-level details, also known as characteristics or minutiae, make each fingerprint unique and form the basis of fingerprint identification. In practical crime identification their unambiguous imaging is critical. Additionally, the third-level details, namely the pores of sweat glands, were also observed (in magnified images 2 and 3) along the papillary ridges. Currently, the third-level details are being used by forensic officers in some countries, in particular in partial fingerprint identification. Seeing the third-level details reflects the advantage of ECL enhancement over those conventional methods involving application of external materials, where the ridges become decorated so that the sweat pores are concealed.

To evaluate the visualization enhancement by local ECL generation, variation of cross-sectional gray values over a few parallel ridges were investigated using ImageJ software, which reads out the pixels and outputs the gray values. The dark ridge defines a lower gray value, while the bright furrow defines a

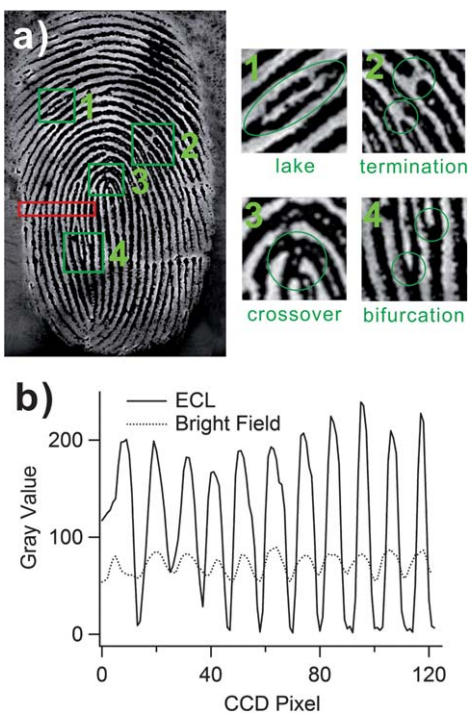

Fig. 3 (a) ECL image of a sebaceous fingerprint deposited on a stainless steel surface obtained at an applied potential of 1.15 V, in which various second level details can be identified. (b) Cross-sectional gray values over 11 parallel papillary ridges as indicated by the red rectangle in (a).

higher value. As shown in Fig. 3b, over 11 parallel ridges, in the bright-field image the cross-sectional gray value from ridge to furrow is slightly different, while it varies significantly in the ECL image. The average difference in the gray value is about 200, suggesting that the fingerprint visualization was enhanced by several tens of times by spatially selective ECL generation. Since the light-emitting species are *in situ* generated close to electrode surfaces, ECL has no background interference and allows temporal and spatial control over the initiation, rate and course of the reaction.[40] Compared with fluorescence methods, ECL images are free of scattered light, luminescent impurities and autofluorescence. Moreover, the specificity of the ECL reaction between $Ru(bpy)_3^{2+}$ and TPrA decreases problems with side reactions, such as self-quenching.[40] In addition, ECL imaging for LFPs visualization offers a fast imaging speed, and the image can be captured immediately upon reaching the appropriate voltage during the CV scan (see Video 1 in the ESI†).

Fig. 4 shows the ECL intensity–potential profile obtained from a stainless steel electrode deposited with a sebaceous fingerprint in 0.01 M PBS containing 0.5 mM $Ru(bpy)_3^{2+}$ and 50 mM TPrA. The ECL emission arises at a potential of 1.08 V, and an ECL peak emerges at a potential of *ca.* 1.25 V. Fig. 5a–f are a collection of CCD images obtained at different applied potentials. Apparently, the appearance of ECL images is in good agreement with the ECL emission profile. At a value far away from the ECL generation potential, *e.g.*, 0.80 V, the image is totally black and does not show any recognizable contrast (Fig. 5a). As the potential was tuned positively, the oxidation of $Ru(bpy)_3^{2+}$ and TPrA took place and the enhancement of the fingerprint started to appear (Fig. 5b–f). When biasing a potential at greater than 1.0 V, characteristic details of the fingerprint became much clear, and eventually ECL images with a good visual contrast and enough resolution were revealed (Fig. 5c and d). An applied potential of 1.15 V was used throughout this study, which was sufficient to achieve good enough visual contrast.

Since ECL intensity is closely dependent on the concentration of the luminophore, ECL images obtained at various $Ru(bpy)_3^{2+}$ concentrations were investigated. As shown in Fig. 6, when the concentration of $Ru(bpy)_3^{2+}$ was lower than 0.5 mM, the ECL was too weak to detect. Only when the concentration was higher than 0.5 mM, could a distinguishable contrast between the fingerprint and the substrate surface be achieved. Therefore, a concentration of $Ru(bpy)_3^{2+}$ at 0.5 mM and that of TPrA at 50 mM were eventually employed for ECL imaging.

The stability and reproducibility of the ECL image was also examined in another control experiment by applying a constant potential excitation for ECL generation. As shown in Fig. 7, upon maintaining a potential at 1.15 V, a concentration of $Ru(bpy)_3^{2+}$ at 0.5 mM and that of TPrA at 50 mM, the ECL image of a sebaceous fingerprint is relatively stable. Over 240 s, the

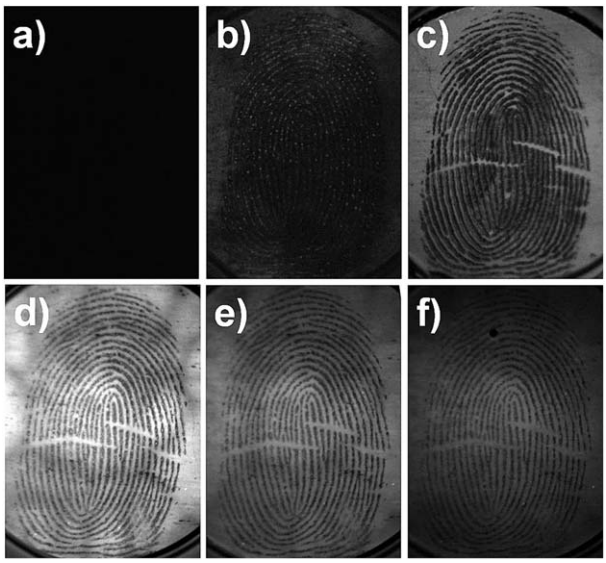

Fig. 5 ECL images of a sebaceous fingerprint deposited on a stainless steel surface obtained at different applied potentials: (a) 0.80 V; (b) 1.0 V; (c) 1.15 V; (d) 1.25 V; (e) 1.30 V; (f) 1.40 V.

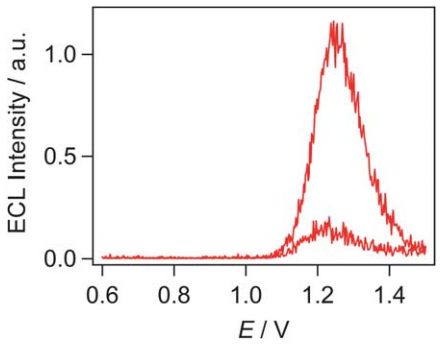

Fig. 4 ECL intensity-potential curve of a stainless steel electrode deposited with a sebaceous fingerprint at a potential scan rate of 0.05 V s^{-1}. The electrolyte solution was 0.01 M PBS containing 0.15 M NaCl, 0.5 mM $Ru(bpy)_3^{2+}$ and 50 mM TPrA.

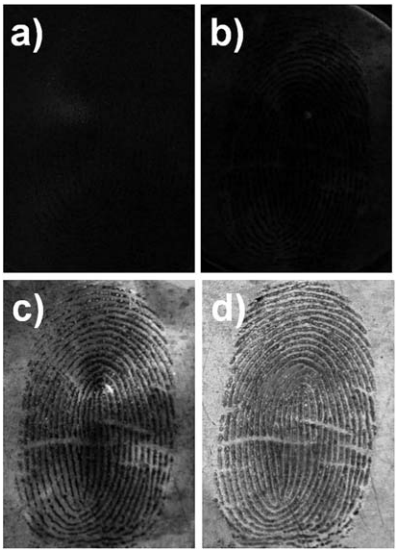

Fig. 6 ECL images obtained at various concentrations of $Ru(bpy)_3^{2+}$ ((a) 0.1 mM, (b) 0.20 mM, (c) 0.50 mM, (d) 1.0 mM) and at an applied potential of 1.15 V. The TPrA concentration was kept at 50 mM.

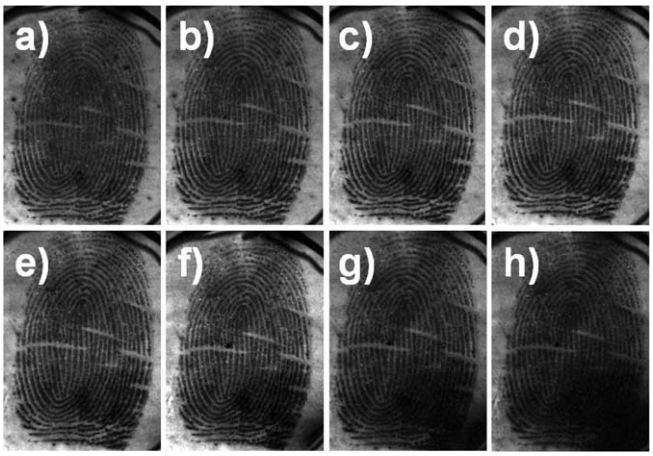

Fig. 7 ECL images of a sebaceous fingerprint obtained as a function of time: (a) 0, (b) 30, (c) 60, (d) 120, (e) 150, (f) 180, (g) 210, (h) 240 s.

resolution of the image remained good. The decay of image brightness could be related to the large consumption of TPrA. After replacing the electrolyte solution, the ECL image can be easily recovered. As shown in Fig. 8, ECL enhancement of the same fingerprint was repeatedly observed upon changing the electrolyte solution. No apparent decay in the ECL image was observed, indicating the non-destructive nature of this method.

We finally demonstrated that the proposed ECL imaging approach could be utilized to enhance sebaceous fingerprints collected from various object surfaces. First, fingerprints deposited on different surfaces were lifted by a short length of double sided adhesive tape. Subsequently, fingerprint materials were released onto the stainless steel surface by softly pressing the tape on the sheet's surfaces. Note that the professional forensic tape or Scotch tape was unfit for such a transfer test due to its strong adhesion, which made it fail to release fingerprint residue onto the stainless steel surface. Fig. 9 shows the ECL images of sebaceous fingerprints transferred onto the stainless steel electrode from four different nonporous surfaces, *i.e.* computer screen, optical disk, laboratory cabinet and coin. The ridge details of the fingerprint are clearly seen in the photographs shown in Fig. 9. Several transfer and detection methods, on the basis of Fourier-transformed infrared spectroscopic, fluorescence spectroscopic techniques and electrospun nanofiber mat, have been reported recently.[41–43] Our further work is in progress to image LFPs on conductive pastes and gels, with which LFPs can be imaged directly after lifting, reducing the loss of fingerprint materials in the releasing step.

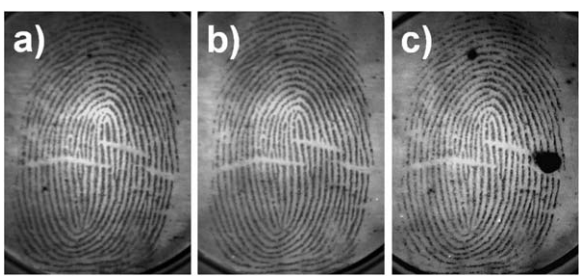

Fig. 8 ECL images of the same sebaceous fingerprint sample obtained upon changing the ECL reaction solution at the first, third, and eighth measurement, respectively.

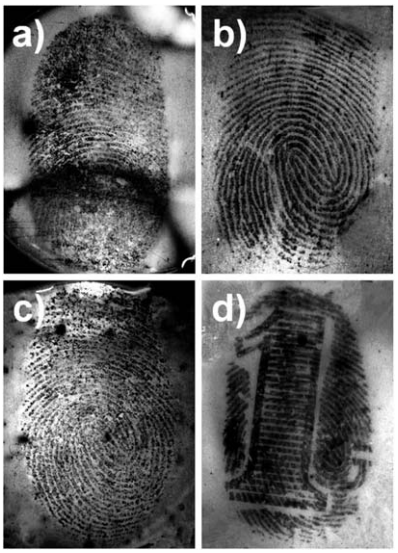

Fig. 9 ECL images of the sebaceous fingerprints collected from different object surfaces: (a) computer screen, (b) optical disk, (c) laboratory cabinet, (d) coin.

Conclusions

A new approach for developing latent fingerprints on stainless steel by ECL enhancement is presented. The method is based on spatial selective control of ECL generation at the electrode surface, which could produce an enhanced visual contrast between the dark ridges and the bright substrate surface. A constant potential of 1.15 V and $Ru(bpy)_3^{2+}$ concentration of 0.5 mM were optimized for a satisfactory enhancement. This approach is rapid, simple, does not need any pre-/post-treatment. Particularly, in comparison with conventional methods reliant on the interaction of developers with fingerprint materials, ECL imaging is non-destructive and therefore does not prevent further chemical identification or DNA analysis. Since identification of LFPs on metallic surfaces is highly important and practically useful at the scene of a crime, we intend to apply this approach to more metal items (such as guns, bullets, knives and keys) that are closely related to serious and organized crimes. Moreover, further studies in progress also include utilizing functionalised or multiple ECL luminophores, for simplifying ECL imaging protocols or exploiting new processes for multiplexed ECL imaging.[44–46]

Acknowledgements

This work is supported by the National Natural Science Foundation of China (21222504) and the Scholarship Award for Excellent Doctoral Student granted by the Ministry of Education.

Notes and references

1 H. C. Lee and R. E. Gaensslen, *Advances in Fingerprint Technology*, CRC Press, Boca Raton, 2nd edn, 2001.
2 M. R. Hawthorne, *Fingerprint Analysis and Understanding*, CRC Press, Boca Raton, 2009.
3 C. Champod, C. Lennard, P. Margot and M. Stoilovic, *Fingerprints and Other Ridge Skin Impressions*, CRC Press, Boca Raton, 2004.
4 R. Leggett, E. E. Lee-Smith, S. M. Jickells and D. A. Russell, *Angew. Chem., Int. Ed.*, 2007, **46**, 4100–4103.
5 P. Hazarika, S. M. Jickells, K. Wolff and D. A. Russell, *Angew. Chem., Int. Ed.*, 2008, **47**, 10167–10170.
6 P. Hazarika, S. M. Jickells and D. A. Russell, *Analyst*, 2009, **134**, 93–96.
7 O. S. Wolfheis, *Angew. Chem., Int. Ed.*, 2009, **48**, 2268–2269.
8 P. Hazarika, S. M. Jickells, K. Wolff and D. A. Russell, *Anal. Chem.*, 2010, **82**, 9150–9154.
9 A. M. Boddis and D. A. Russell, *Anal. Methods*, 2011, **3**, 519–523.
10 X. Spindler, O. Hofstetter, A. M. McDonagh, C. Roux and C. Lennard, *Chem. Commun.*, 2011, **47**, 5602–5604.
11 A. M. Boddis and D. A. Russell, *Anal. Methods*, 2012, **4**, 637–641.
12 P. Hazarika and D. A. Russell, *Angew. Chem., Int. Ed.*, 2012, **51**, 3524–10.
13 M. Wood, P. Maynard, X. Spindler, C. Lennard and C. Roux, *Angew. Chem., Int. Ed.*, 2012, **51**, 12272–12274.
14 V. Bowman, *Fingerprint Development Handbook*, Heanor Gate Printing Limited, Heanor, Derbyshire, UK, 2nd edn, 2005.
15 P. V. Haan, *Contemp. Phys.*, 2006, **47**, 209–230.
16 N. Jones, M. Stoilovic, C. Lennard and C. Roux, *Forensic Sci. Int.*, 2001, **123**, 5–12.
17 X. Dai, M. Stoilovic, C. Lennard and N. Speers, *Forensic Sci. Int.*, 2007, **168**, 219–222.
18 J. Fraser, K. Sturrock, P. Deacon, S. Bleay and D. H. Bremner, *Forensic Sci. Int.*, 2011, **208**, 74–78.
19 I. H. Yu, S. Jou, C. Chen, K. Wang, L. Pang and J. S. Liao, *Forensic Sci. Int.*, 2011, **207**, 14–18.
20 N. Jaber, A. Lesniewski, H. Gabizon, S. Shenawi, D. Mandler and J. Almog, *Angew. Chem., Int. Ed.*, 2012, **51**, 12224–12227.
21 C. Bersellini, L. Garofano, M. Giannetto, F. Lusardi and G. Mori, *J. Forensic Sci.*, 2001, **46**, 871–877.
22 A. L. Beresford and A. R. Hillman, *Anal. Chem.*, 2010, **82**, 483–486.
23 A. L. Beresford, R. M. Brown, A. R. Hillman and J. W. Bond, *J. Forensic Sci.*, 2012, **57**, 93–102.
24 R. M. Brown and A. R. Hillman, *Phys. Chem. Chem. Phys.*, 2012, **14**, 8653–8661.
25 L. Xu, Y. Li, S. Wu, X. Liu and B. Su, *Angew. Chem., Int. Ed.*, 2012, **51**, 8068–8072.
26 G. Williams and N. McMurray, *Forensic Sci. Int.*, 2007, **167**, 102–109.
27 X. N. Shan, U. Patel, W. S. P. R. Iglesias and N. J. Tao, *Science*, 2010, **327**, 1363–1366.
28 M. Q. Zhang, A. Becue, M. Prudent, C. Champod and H. H. Girault, *Chem. Commun.*, 2007, 3948–3950.
29 M. Q. Zhang and H. H. Girault, *Electrochem. Commun.*, 2007, **9**, 1778–1782.
30 M. Q. Zhang and H. H. Girault, *Analyst*, 2009, **134**, 25–30.
31 G. Qin, M. Zhang, T. Zhang, Y. Zhang, M. McIntosh, X. Li and X. Zhang, *Electroanalysis*, 2012, **24**, 1027–1032.
32 G. Williams, N. McMurray and D. A. Worsley, *J. Forensic Sci.*, 2001, **46**, 1085–1092.
33 R. K. Bentsen, J. K. Brown, A. Dinsmore, K. K. Harvey and T. G. Kee, *Sci. Justice*, 1996, **36**, 3–8.
34 Y. Migron, G. Hocherman, E. Springer, J. Almog and D. Mandler, *J. Forensic Sci.*, 1998, **43**, 543–548.
35 Y. Migron and D. Mandler, *J. Forensic Sci.*, 1997, **42**, 986–992.
36 A. A. Cantu, D. A. Leben, R. Ramotowski, J. Kopera and J. R. Simms, *J. Forensic Sci.*, 1998, **43**, 294–298.
37 F. Schutz, M. Bonfanti and C. Champod, *Can. Soc. Forensic Sci. J.*, 2000, **33**, 65–81.
38 R. Reed, *Ident News*, 1985, **35**, 11.
39 G. Kwak, W. Lee, W. Kim and H. Lee, *Chem. Commun.*, 2009, 2112–2114.
40 W. Miao, *Chem. Rev.*, 2008, **108**, 2506–2553.
41 C. Ricci, S. Bleay and S. G. Kazarian, *Anal. Chem.*, 2007, **79**, 5771–5776.
42 G. Kwak, W.-E. Lee, W.-H. Kim and H. Lee, *Chem. Commun.*, 2009, 2112–2114.
43 S. Yang, C. Wang and S. Chen, *Angew. Chem., Int. Ed.*, 2011, **50**, 3706–3709.
44 K. N. Swanick, S. Ladouceur, E. Zysman-Colman and Z. Ding, *Angew. Chem., Int. Ed.*, 2012, **51**, 11079–11082.
45 E. H. Doeven, E. M. Zammit, G. J. Barbante, C. F. Hogan, N. W. Barnett and P. S. Francis, *Angew. Chem., Int. Ed.*, 2012, **51**, 4354–4357.
46 E. H. Doeven, E. M. Zammit, G. J. Barbante, P. S. Francis, N. W. Barnett and C. F. Hogan, *Chem. Sci.*, 2013, **4**, 977–982.

